Subnatural Linewidth Single Photons from a Quantum Dot

Clemens Matthiesen,[1,*] Anthony Nickolas Vamivakas,[1,2] and Mete Atatüre[1,†]

[1]*Cavendish Laboratory, University of Cambridge, JJ Thomson Avenue, Cambridge CB3 0HE, United Kingdom*
[2]*Institute of Optics, University of Rochester, 275 Hutchison Road, Rochester, New York 14627-0186, USA*

(Received 15 September 2011; revised manuscript received 13 February 2012; published 28 February 2012)

The observation of quantum-dot resonance fluorescence enabled a new solid-state approach to generating single photons with a bandwidth approaching the natural linewidth of a quantum-dot transition. Here, we operate in the small Rabi frequency limit of resonance fluorescence—the Heitler regime—to generate subnatural linewidth and high-coherence quantum light from a single quantum dot. The measured single-photon coherence is 30 times longer than the lifetime of the quantum-dot transition, and the single photons exhibit a linewidth which is inherited from the excitation laser. In contrast, intensity-correlation measurements reveal that this photon source maintains a high degree of antibunching behavior on the order of the transition lifetime with vanishing two-photon scattering probability. Generating decoherence-free phase-locked single photons from multiple quantum systems will be feasible with our approach.

DOI: 10.1103/PhysRevLett.108.093602 PACS numbers: 87.64.kv, 03.67.−a, 42.50.Ar, 81.07.Ta

Numerous proposals in quantum information science ranging from distributed entanglement generation to interfacing disparate qubits rely on single-photon generation from state-selective optical transitions [1–4]. The full quantum description of the resonant interaction of a two-level system with light is captured in the statistical and spectral properties of the scattered light. Shortly after a number of theoretical investigations [5–7], quantum effects were observed in the spectra and photon correlations of atomic-beam resonance fluorescence (RF) [8–10]. RF is now routinely employed in optical investigations of atomic gases, single trapped ions, and atoms [11]. In the large Rabi frequency limit, the RF spectrum develops into the Mollow triplet [5]. In this regime, the generated photons are antibunched on the time scale of the excited-state lifetime, they bear no phase relation to the excitation field, and their coherence is constrained to the antibunching time scale. Conversely, in the small Rabi frequency limit, two otherwise independent processes of absorption and emission become a single coherent event. In such a process, the scattered photon spectrum replicates the excitation field exhibiting comparable first-order optical coherence. The same scattered field also displays strong antibunching in photon correlation measurements. This phenomenon, known as the Heitler effect [12], has been demonstrated in trapped ions using heterodyning [13] and spectral measurement [14,15] techniques.

RF has only recently been observed from solid-state emitters, such as dye molecules [16] and self-assembled quantum dots (QDs) [17–20]. The strictly resonant excitation was shown to minimize photonic decoherence when compared to nonresonant excitation [21–25] approaching the radiative lifetime limit. Further, taking advantage of the spin-selective QD transitions, required for spin-based quantum information science [26], QD RF allowed detailed studies of spin dynamics [27,28], excitation-induced sideband broadening [29], and the realization of single-shot spin readout [30]. Surprisingly, the limit of vanishing Rabi frequency in the resonant interaction has remained relatively unexplored for atoms, ions, and any single solid-state emitter [31]. The technical challenge to observe the elastically scattered photons is to suppress sufficiently the laser background and the incoherent component of RF. Here, we demonstrate that, in the limit of the Rabi frequency much smaller than the spontaneous emission rate—the Heitler regime [12], the spectrum and the coherence properties of RF photons are liberated from the QD transition properties and are tailored predominantly by the excitation laser properties. In other words, a quantum dot generates single photons with laserlike coherence free from any dephasing processes affecting the QD light emission.

Our experimental arrangement constitutes a confocal microscope operating at 4 K where the combination of cross-polarization and confocal rejection of the collection fiber suppresses any residual laser by a factor of 10^7 with respect to the collected RF [32]. Figures 1(a)–1(d) present excitation power dependence of the integrated RF spectrum from a QD transition in order to quantify both the collection efficiency of our system and the fraction of residual laser background in the detected photons. In panel (a), the laser frequency is fixed and photodetection events are recorded (open circles) as a function of gate bias (the bias Stark shifts the QD transition). The full-width half-maximum (FWHM) of the Lorentzian curve fit to the data is 530 MHz in linear frequency for the excitation power at the saturation point. The inset displays the residual background for large detunings (dark bars) including the contribution of single-photon counting

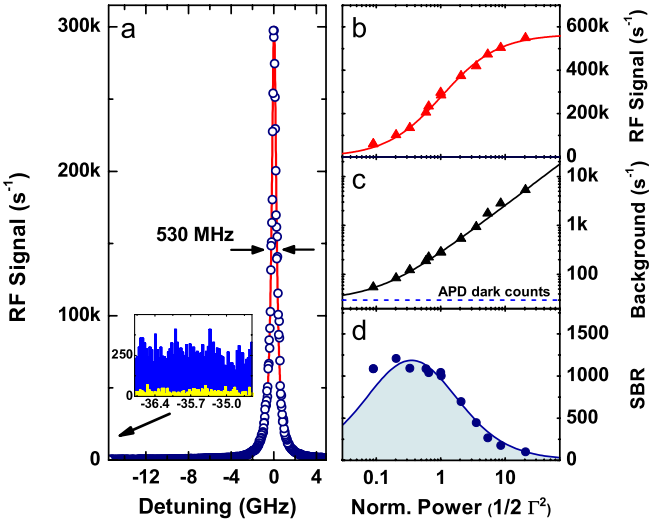

FIG. 1 (color online). Collection efficiency and background analysis of RF. (a) Integrated photon counts for RF at the saturation point as a function of laser detuning. The curve is a Lorentzian fit to the data (open circles). Inset: Total off-resonance (detuned by 35 GHz) background counts (dark) compared to the APD dark counts alone (light). (b) Integrated photon detection events when the laser is on-resonance with the QD transition and (c) off-resonance. (d) RF SBR. At saturation ($\Omega \sim \Gamma/\sqrt{2}$) a value of 1050 is achieved. The excitation power for (b)-(d) is scaled in units of the saturation power $\Omega^2 = \Gamma^2/2$.

avalanche photodiode (APD) dark counts (yellow bars). In panels (b) and (c), the triangles display the total photodetection events per second on and off resonance, respectively, as a function of excitation power normalized to the saturation power. The solid curves represent the theoretically expected fits for the data in each panel. The dashed line indicates the mean dark count level. For an excitation power at the saturation point ($\Omega \sim \Gamma/\sqrt{2}$, where Ω denotes the Rabi frequency and Γ denotes the spontaneous emission rate) we collect approximately 1.25×10^6 photons per second from RF into our single-mode optical fiber, while the laser and detector background contribute $\sim$0.084% of the total signal. With a detector quantum efficiency of approximately 24% we register 3×10^5 detector clicks per second. The filled circles in panel (d) show the obtained ratio of the RF signal to total background (SBR) for each laser power along with the expected power dependence (solid curve). At a tenth of saturation, the residual laser contribution to the background falls below the dark count level limiting the SBR. This degree of RF collection already compares with that obtained from single trapped ions and will allow an increase of electron spin readout fidelity [30] to better than 99% within $30 - \mu$ sec detection time.

The theoretically expected spectrum of RF in the presence of dephasing when the laser is exactly resonant can be given as [20]

$$S(\Delta\nu) \propto \frac{1}{2}\frac{\tilde{T}_2^{-1}}{\Delta\nu^2 + \tilde{T}_2^{-2}} + \frac{1}{2}\frac{1}{(\tilde{T}_1\tilde{T}_2)^{-1} + \Omega^2} \times \left(\frac{A\eta/2 - (8\mu)^{-1}(\Delta\nu - \mu)B}{(\Delta\nu - \mu)^2 + \eta^2} + \frac{A\eta/2 + (8\mu)^{-1}(\Delta\nu + \mu)B}{(\Delta\nu + \mu)^2 + \eta^2}\right) + \frac{1}{\tilde{T}_1\tilde{T}_2^{-1} + \Omega^2\tilde{T}_1^2}\delta(\Delta\nu), \quad (1)$$

where $\Delta\nu$ is the detuning in linear frequency, $\tilde{T}_1$ and $\tilde{T}_2$ are lifetime and dephasing time, Ω is the Rabi frequency. A, B, μ, and η are $A = \Omega^2 + (\tilde{T}_1^{-1} - \tilde{T}_2^{-1})\tilde{T}_1^{-1}$, $B = 2\Omega^2 + (3\tilde{T}_1^{-1} - \tilde{T}_2^{-1}) - 2(\tilde{T}_1^{-1} - \tilde{T}_2^{-1})^2\tilde{T}_1^{-1}$, $\mu = \sqrt{\Omega^2 - 1/4(\tilde{T}_1^{-1} - \tilde{T}_2^{-1})^2}$, and $\eta = (\tilde{T}_1^{-1} + \tilde{T}_2^{-1})/2$. The first three terms of Eq. (1) originate from the incoherent component while the last term is responsible for the coherently scattered photons. At high excitation power the incoherent component reveals the Mollow triplet, while at low excitation power the spectrum is dominated by the coherent part. Figures 2(a)–2(c) display the measured spectrum of quantum-dot RF for three excitation power settings $-\Omega \sim 1.5\Gamma$, $\Omega \sim 0.6\Gamma$, $\Omega \sim 0.22\Gamma$, respectively. Here the laser is fixed on-resonance with the QD transition and the RF spectrum is recorded through a scanning Fabry-Perot cavity (FWHM $\sim$29 MHz). The measured spectrum (filled circles) in panel (a) displays the expected Mollow triplet together with a subnatural linewidth peak due to the coherently scattered component along with the theoretically expected line shape for each component (solid curves). The fits are obtained by convolving Eq. (1) with the Fabry-Perot cavity bandwidth [32]. The incoherent part dominates the deconvolved spectrum in panel (a). In panel (b), both coherent and incoherent components are still visible, but the incoherent component is reduced to a single peak. Figure 2(c) displays the same measurement for a lower excitation power ($\Omega \sim 0.22\Gamma$), where the entire measured spectrum collapses to a Fabry-Perot cavity resolution-limited subnatural linewidth Lorentzian. Any residual incoherent component of RF in this regime is less than the detectable level within the spectral resolution and the signal-to-noise ratio of our measurements. We note that detuning the excitation laser from the QD transition provides another way of tuning the ratio of coherent to incoherent components increasing the coherent scattering component [32].

Figures 2(d)–2(f) display the intensity-correlation measurements performed on the complete RF emission at the three Rabi frequency settings of Figs. 2(a)–2(c) using a Hanbury Brown–Twiss setup. The raw data for each measurement decorate the theoretically expected function (dotted curve) and its convolution with the measured instrument response function [32] (solid curve). In Panel (d), the onset of Rabi oscillations is visible in the

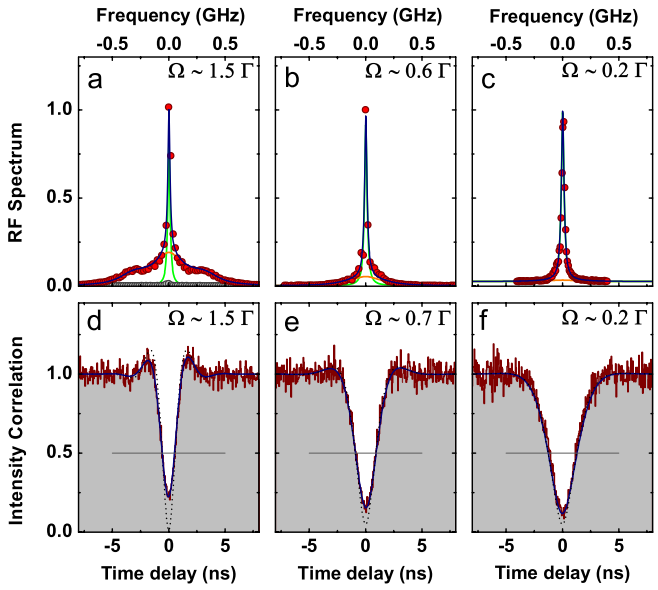

FIG. 2 (color online). Spectrum and intensity-correlation measurements on QD RF. (a) A narrowband single-mode laser is fixed on-resonance with the QD transition at $\Omega \sim 1.5\Gamma$ and the RF spectrum is recorded by an APD as the transmission through a scanning Fabry-Perot cavity (FWHM ~29 MHz), shown as filled circles. The spectrum (fitted with the solid curve) comprises the onset of the Mollow triplet superimposed by the coherently scattered component. The open circles display the residual laser background under the same conditions, but when the QD transition is gate-detuned. (b) Same measurement as panel (a) performed when the laser power is around saturation ($\Omega \sim 0.6\Gamma$) and (c) when the laser power is below saturation ($\Omega \sim 0.2\Gamma$). The spectrum collapses to a single Lorentzian of width indistinguishable from the resolution of the scanning cavity. The offset is caused by detector dark counts and ambient light. (d)–(f) Intensity-correlation measurements of RF for the excitation power regimes of the spectra presented in panels (a)–(c), respectively. In all the plots the data are superimposed by the theoretical prediction (continuous curves) convolved with the system response function [32], while the dotted black lines indicate how our measurements would appear for an ideal system response. All plots display the ubiquitous antibunching behavior at zero time delay.

intensity-correlation function, which exhibits an oscillatory behavior in addition to strong antibunching [$g^2(0) = 0.01 \pm 0.01$ after deconvolution]. Antibunching is sustained fully on the time scale of the excited-state lifetime $T_1 = 760$ ps for lower Rabi frequencies in panels (e) and (f). While the dramatic linewidth narrowing observed in panel (c) suggests the wave nature of light is maintained over time scales significantly beyond the excited-state lifetime, the intensity-correlation measurements dictate that the particlelike nature of the photons is preserved even in this regime.

To obtain a more precise value for the photon emission linewidth, we employ field-correlation measurements using a Michelson interferometer [32]. As a lower bound for single-photon coherence, the circles in Fig. 3(a) display the interference fringe visibility for QD emission under low power incoherent excitation. The resulting coherence time is ~540 ps, which is substantially shorter than 1.52 ns—the theoretical upper limit of $T_2 = 2T_1$ for the investigated QD—and is consistent with recent reports on the modest degree of two-photon interference from independent QDs [33,34]. The dotted line in Fig. 3(a) represents the measured fringe visibility for the laser and limits the maximum attainable coherence time in our experiments to ~50 ns. The squares display the fringe visibility for RF generated at $\Omega \sim 0.2\Gamma$—the same condition as for Figs. 2(c) and 2(f). The fit to Eq. (1) which includes both incoherent and coherent components sets the coherence time of the incoherent emission to, within the measurement uncertainty, $2T_1$. It also allows us to extract the fraction of incoherent to total scattering of ~11%. For the coherent component on the other hand the fit yields a coherence time of 22 ns, or equivalently a linewidth of at most 7 MHz: this coherence time is at least 15 times longer than the theoretical limit of coherence for spontaneously emitted photons, where absorption and emission can be considered as two separate physical events. This is 30 times longer than

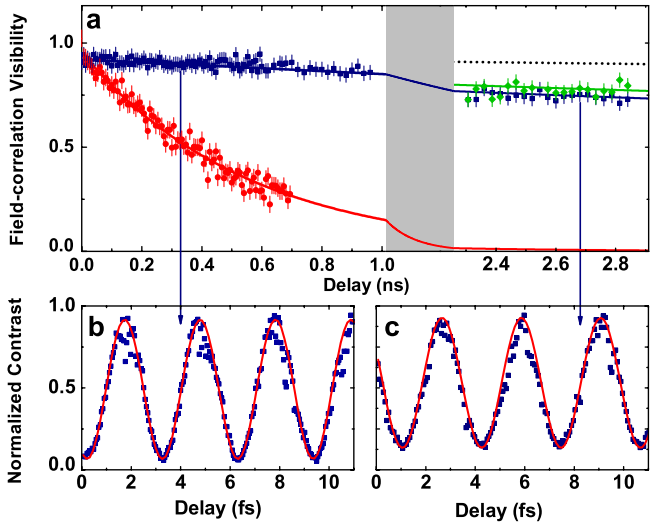

FIG. 3 (color online). First-order correlation measurement of QD RF. (a) The visibility of the interference fringes observed for RF for the laser excitation power corresponding to $\Omega \sim 0.22\Gamma$ (squares) and $\Omega \sim 0.17\Gamma$ (diamonds). The dotted line is the measured mean fringe visibility for the laser and marks the highest attainable coherence of the scattered photons. The first-order correlation measurement for incoherently generated photons (above GaAs band gap excitation) (circles) shows a coherence time of ~540 − ps, while the RF displays a coherence time of ~22 ns in the Heitler limit, i.e., ~15 times longer than the antibunching time scale. The detailed description of the theoretical fits to the data (solid curves) can be found in the Supplemental Material [32]. (b) A close-up of the raw interference fringes for $\Omega \sim 0.22\Gamma$ for a relative time delay of 330 ps. The fringe visibility here is 0.90. (c) Same as panel (b) for a relative time delay of 2.68 ns and visibility of 0.75.

the lifetime of the QD transition. The reported coherence time constitutes an upper bound on the coherence of individual photons as spectral wandering (few MHz) of the narrowband laser on the time scale of the measurement washes out the interference fringe contrast. At even lower excitation power [$\Omega \sim 0.17\Gamma$, data as diamonds in Fig. 3(a)] the incoherent fraction further reduces to $\sim 7\%$. In this regime the interference fringe visibility of RF after a delay of ~ 2.6 ns is as high as 85% of that displayed by the coherent laser. Examples of measured interference fringes for $\Omega \sim 0.2\Gamma$ for two time delays are shown in Figs. 3(b) and 3(c).

These results reveal the counterintuitive nature of RF in the Heitler regime: The QD operates as a quantum converter of a weak coherent state into a coherent single-photon stream. The photons arrive one at a time to our detection system, but are phase-correlated with each other and with the laser field from which they originated. In this regime, issues thought to be inherent in solid-state systems, such as spectral diffusion, modify the probability to scatter a photon, but do not cause photon decoherence due to the absence of an exciton interacting with the environment.

In this work we have demonstrated that a solid-state quantum emitter such as a single QD can generate single photons with bandwidth and coherence that are tailored by the excitation laser. Consequently, an immediate opportunity emerges where tunable and time-synchronized single photons can be generated from multiple QDs with near-arbitrarily tailored spectral and phase properties using the same excitation laser. Photons generated in the Heitler regime from multiple sources will be phase-locked to the excitation laser and, hence, to each other. In contrast to using an ultrafast pulse to trigger an excited-state population [21,22] for single photons, our approach lends itself to the use of nanosecond pulses where there is significant technical ease in controlling the amplitude and phase of the excitation field. Such custom-designed photonic states will facilitate high-fidelity photonic coupling between otherwise disparate quantum systems, such as spectrally distinct QDs and trapped ions [4], as required for the realization of distributed hybrid quantum networks [1].

This work was supported by grants and funds from the University of Cambridge, EPSRC Science and Innovation Grant, the QIPIRC and EPSRC Grant No. EP/G000883/1. We thank C. Stroud, Jr., M. Kohl, and Z. Hadzibabic for useful discussions, and P. Humphreys, C.-Y. Lu, and G. Winiecki for technical assistance. We further thank M. Hugues, M. Hopkinson, and the National Centre for III–V Technologies for providing the QD sample used in this work.

During the reviewing process of our manuscript, we became aware of Ref. [35] reporting similar results.

*cm467@cam.ac.uk
†ma424@cam.ac.uk

[1] H. J. Kimble, Nature (London) **453**, 1023 (2008).
[2] J. I. Cirac, P. Zoller, H. J. Kimble, and H. Mabuchi, Phys. Rev. Lett. **78**, 3221 (1997).
[3] S. C. Benjamin, B. W. Lovett, and J. M. Smith, Laser Photon. Rev. **3**, 556 (2009).
[4] E. Waks and C. Monroe, Phys. Rev. A **80**, 062330 (2009).
[5] B. R. Mollow, Phys. Rev. **188**, 1969 (1969).
[6] M. D. Crisp and E. T. Jaynes, Phys. Rev. **179**, 1253 (1969).
[7] C. R. Stroud, Jr., Phys. Rev. A **3**, 1044 (1971).
[8] F. Schuda, C. R. Stroud, Jr., and M. Hercher, J. Phys. B **7**, L198 (1974).
[9] F. Y. Wu, R. E. Grove, and S. Ezekiel, Phys. Rev. Lett. **35**, 1426 (1975).
[10] H. J. Kimble, M. Dagenais, and L. Mandel, Phys. Rev. Lett. **39**, 691 (1977).
[11] D. Leibfried, R. Blatt, C. Monroe, and D. Wineland, Rev. Mod. Phys. **75**, 281 (2003).
[12] W. Heitler, *The Quantum Theory of Radiation* (Clarendon Press, Oxford, 1954).
[13] J. T. Hoffges, H. W. Baldauf, T. Eichler, S. R. Helmfrid, and H. Walther, Opt. Commun. **133**, 170 (1997).
[14] H. M. Gibbs and T. N. C. Venkatesan, Opt. Commun. **17**, 87 (1976).
[15] J. Volz, M. Weber, D. Schlenk, W. Rosenfeld, C. Kurtsiefer, and H. Weinfurter, Laser Phys. **17**, 1007 (2007).
[16] G. Wrigge, I. Gerhardt, J. Hwang, G. Zumofen, and V. Sandoghdar, Nature Phys. **4**, 60 (2007).
[17] A. Muller *et al.*, Phys. Rev. Lett. **99**, 187402 (2007).
[18] R. Melet *et al.*, Phys. Rev. B **78**, 073301 (2008).
[19] A. N. Vamivakas *et al.*, Nature Phys. **5**, 198 (2009).
[20] E. B. Flagg *et al.*, Nature Phys. **5**, 203 (2009).
[21] J. Kim, O. Benson, H. Kan, and Y. Yamamoto, Nature (London) **397**, 500 (1999).
[22] P. Michler *et al.*, Science **290**, 2282 (2000).
[23] C. Santori, D. Fattal, J. Vuckovic, G. S. Solomon, and Y. Yamamoto, Nature (London) **419**, 594 (2002).
[24] A. Kiraz, M. Atatüre, and A. Imamoglu, Phys. Rev. A **69**, 032305 (2004).
[25] S. Ates *et al.*, Phys. Rev. Lett. **103**, 167402 (2009).
[26] A. Imamoglu *et al.*, Phys. Rev. Lett. **83**, 4204 (1999).
[27] C. L. Lu *et al.*, Phys. Rev. B **81**, 035332 (2010).
[28] P. Fallahi, S. T. Yilmaz, and A. Imamoglu, Phys. Rev. Lett. **105**, 257402 (2010).
[29] S. M. Ulrich *et al.*, Phys. Rev. Lett. **106**, 247402 (2011).
[30] A. N. Vamivakas *et al.*, Nature (London) **467**, 297 (2010).
[31] H. Stolz, Phys. Status Solidi B **234**, 107 (2002).
[32] See Supplemental Material at http://link.aps.org/supplemental/10.1103/PhysRevLett.108.093602 for additional data, description, and analysis of results in this Letter.
[33] E. B. Flagg *et al.*, Phys. Rev. Lett. **104**, 137401 (2010).
[34] R. B. Patel *et al.*, Nature Photon. **4**, 632 (2010).
[35] H. S. Nguyen *et al.*, Appl. Phys. Lett. **99**, 261904 (2011).